Colloid Polym Sci (2007) 285:673–680
DOI 10.1007/s00396-006-1612-6

ORIGINAL CONTRIBUTION

Concentrated reverse micelles in a random graft block copolymer system: structure and in-situ synthesis of silver nanoparticles

Carlos Rodríguez-Abreu · Massimo Lazzari · Dharmesh Varade · Masaya Kaneko · Kenji Aramaki · Manuel Arturo López Quintela

Received: 29 September 2006 / Accepted: 17 October 2006 / Published online: 1 December 2006

Abstract The structure and rheological properties of a poly (dimethylsiloxane)-graft-poly(oxyethylene) copolymer at high concentrations in block-selective solvents were studied by small-angle X-ray scattering (SAXS) and rheometry. Analysis of SAXS data indicates that quasispherical, reverse micellar aggregates (with no ordered packing) are present in concentrated solutions of the copolymer in nonpolar solvents, and that upon addition of water, the size of such aggregates increases due to the solubilization inside the micellar cores. The viscosity of concentrated polymer solutions increases exponentially as water is added, and finally, viscoelastic, gel-like behavior is found in the vicinity of the phase separation limit. It was found that small silver nanoparticles with an average diameter of ≈3 nm can be synthesized inside the copolymer aggregates without the need of a reducing agent; namely, particles embedded in a viscoelastic matrix are obtained. The synthesis seems to follow first-order kinetics.

Keywords Small-angle X-ray scattering (SAXS) · Rheology · Reverse micelles · Organogels · Silver nanoparticles · Block copolymers

Electronic supplementary material Supplementary material is available in the online version of this article at http://dx.doi.org/10.1007/s00396-006-1612-6 and is accessible for authorized users.

C. Rodríguez-Abreu (✉) · M. Lazzari · M. A. López Quintela
Departamento de Química Física, Facultad de Química,
Universidad de Santiago de Compostela,
Santiago de Compostela 15782, Spain
e-mail: carlosetsuko@yahoo.com

D. Varade · M. Kaneko · K. Aramaki
Graduate School of Environment and Information Sciences,
Yokohama National University,
Tokiwadai 79-7,
Hodogaya-ku, Yokohama 240-8501, Japan

Introduction

Siloxane amphiphilic copolymers are surface-active in both aqueous and nonaqueous media and can reduce the surface tension up to 20 mN/m because the poly(dimethylsiloxane) (PDMS) chains have low cohesive energy. Moreover, since Si–O–Si bonds are very flexible, siloxane amphiphilic copolymers are fluid even at very high molecular weights [1] and they do not generally show a Krafft point or a gel point in aqueous media [2]. They also have the capability of forming reverse aggregates and lyotropic and thermotropic liquid crystals, such as reverse hexagonal and cubic phases, in nonaqueous media [3–5]. Typical siloxane amphiphilic copolymers consist of a methylated siloxane hydrophobe grafted with one or more polar chains, such as poly (oxyalkylene). Depending on the relative length of the blocks, those copolymers can form micellar aggregates in dilute aqueous solutions [6, 7], but there are few studies on the phase behavior of concentrated systems [8].

Due to the features mentioned above, siloxane amphiphilic copolymers are used in a wide variety of applications, including foam stabilization in plastic (polyurethane) foams, cosmetics, wetting, emulsification, lubrication and antistatic agents, drug delivery, and so forth [9–13]. Therefore, it is relevant to know the relationships between functionality and structure. In cosmetics, for example, viscoelasticity is an important property that should be characterized. As mentioned above, siloxane copolymers form aggregates in nonaqueous media, but little has been reported on the relationship between nanostructure and rheological properties of such systems [14], as well as on their potential use as nanoreactors [15]. Micellar cores may be loaded with inorganic precursors and then processed to produce nanoparticles, in a similar way as it is also done with amphiphilic block copolymers [16, 17].

On the other hand, there is growing interest in using additives at the nanoscale level to enhance the functions of commercial products. For example, silver nanoparticles offer promises as antibacterial agents and optical filters; therefore, it is important to assess the effect of incorporating nanoparticles on properties relevant for practical applications. Although there are studies on the use of block copolymers as media for the preparation and stabilization of silver nanoparticles [18–20], to our knowledge, there is no report on the use of siloxane copolymer concentrated solutions as hosts for the synthesis of metallic nanoparticles.

In a previous paper [8], the formation of reverse micellar gels in a concentrated PDMS–poly(ethylene oxide) (PEO) graft block copolymer system was reported, but their structure and rheological behavior were not studied in detail. Here we present results on the self-organization and rheological behavior of concentrated PDMS–PEO graft block copolymer systems and their use as reaction media for the synthesis of silver nanoparticles.

Experimental

Materials

A commercial PDMS-*graft*-PEO, traded under the name SH3775M, was obtained from Dow Corning Toray Silicone (Tokyo, Japan). Molecular and structural characterization were carried out by size exclusion chromatography and ^{1}H NMR, respectively (see supporting information). SH3775M has a weight average molecular weight of 10,800 g/mol and a polydispersity index of 1.5, whereas the approximate molecular formula resulting from NMR-determined molecular composition is shown in Fig. 1. Octamethylcyclotetrasiloxane (designated as D_4) and decane were purchased from Tokyo Kasei Kogyo (Tokyo, Japan). Silver nitrate was obtained from Sigma-Aldrich (St. Louis, MO, USA). All substances were used as received. Deionized water was used in the experiments.

Preparation of the samples

After adding the components, samples were mixed in sealed ampoules with a narrow constriction by alternate centrifugation at 25 °C. The ampoules were left for 24 h in a thermostated bath at 25 °C before small-angle X-ray scattering (SAXS) and rheological measurements. The SH3775M/oil weight ratios were kept at 77/23 in all experiments, a composition at which reverse micelles are formed according to a previously reported phase diagram [8].

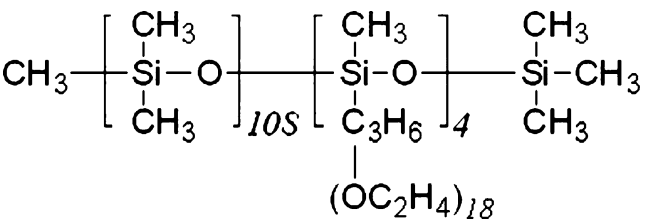

Fig. 1 Molecular formula of SH3775M

Silver nanoparticles were prepared by replacing water with $AgNO_3$ aq. (0.03 M) and using the same mixing procedure described above. No reducing agent was added.

Small-angle X-ray scattering (SAXS)

SAXS measurements were performed at 25 °C by using a SAXSess camera (Anton Paar, PANalytical, Graz, Austria), using a PW3830 laboratory X-ray generator with a long fine focus sealed glass X-ray tube (K_α wavelength of λ=0.1542 nm), operated at 40 kV and 50 mA. The instrument is equipped with multilayer optics, a block collimator, and a semitransparent beam stopper. The scattered intensity was detected by an image plate detector and the recorded intensity was read by a Cyclone storage phosphor system (Perkin Elmer, Norwalk, CT, USA). The solvent scattering was subtracted by using the Primary Data Handling program (Institute of Chemistry, Graz, Austria). Details on the used equations can be found in the supporting information.

UV spectrometry

UV spectra were collected using a Shimadzu UV-2550 UV-visible spectrophotomer. For viscosities lower than 1,000 Pa/s, samples were directly placed in quartz cuvettes for the measurement, whereas for higher viscosities, samples were diluted in ethanol. Samples without added $AgNO_3$ were used as blanks.

Rheological measurements

Measurements were performed in an ARES7 rheometer (Rheometric Scientific, Piscataway, NJ, USA) using both Couette and cone-plate geometry (ϕ=25 mm; cone angle= 0.1 rad). Dynamic frequency sweep measurements were performed in the linear viscoelastic regime, determined in advance by dynamic strain sweep measurements.

Results and discussion

Characterization of graft block copolymer system

The SAXS spectra of SH3775M–D_4–water systems are shown in Fig. 2. In the absence of water, the scattering intensity varies in nonmonotonic fashion with respect to the scattering angle, as when discrete micellar-like aggregates

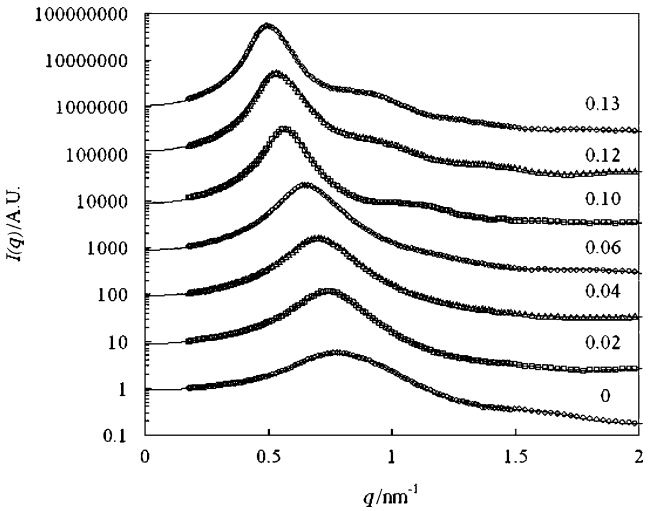

Fig. 2 Desmeared SAXS curves for SH3775M–D_4–water systems at 25 °C for different volume fractions of water (indicated above each *curve*). The *full lines* are the fitting curves obtained by GIFT using the hard-sphere structure factor model. Each *curve* is displaced on the ordinate by a factor of 10 for clarity. The SH3775M/D_4 volumetric ratio is 76/24

embedded in a continuous medium (hydrophobic in this case) are present. Namely, the segregation of PEO chains induces the formation of defined nanodomains. However, only one broad peak can be resolved, indicating the absence of structures with well defined order, namely, the system is not in a liquid crystalline state. As water is added to the system, the position of this peak shifts to smaller scattering vectors and its intensity and sharpness increase. This could suggest an increase in the mean distance between aggregates, as well as in the interactions between them. Nevertheless, water addition does not induce the appearance of high-order reflections; namely, there is no evidence of liquid crystal formation.

In our system we can expect the micellar corona to have a low contrast for X-rays because PDMS and D_4 have similar electron densities; therefore, the highest contribution to the scattering should come from the strongly segregated PEO micellar cores.

From X-ray diffraction spectra in the wide angle range (see supporting information) two broad peaks can be identified at low water contents, one at q=8.4 nm^{-1} and the other at q=15 nm^{-1}. The low-q reflection can be related to that found for PDMS [21, 22], whereas the high-q reflection could be assigned to PEO chains [23]. The broadness of the peaks indicates that the chains are in a disordered, liquid-like state. As water is added to the system, the PEO peak seems to shift to lower q values and merge with the PDMS peak. It indicates an increase in the correlation length associated with the hydration of PEO chains by water solubilization. On the other hand, the position of the peak related to the PDMS chain remains unchanged regardless of hydration; hence, it seems that water has no detectable effect (as far as wide-angle X-ray scattering is concerned) on the conformation of hydrophobic chains.

Analysis of $S(q)$ with the Hard Sphere + Percus-Yevick (HS+PY) model based on the Generalized Indirect Fourier Transform (GIFT) method allows us to estimate the hard-sphere volume fraction, Φ, the interaction radius, $\sigma/2$, and the polydispersity parameter, D (with the limitations inherent to the HS–PY model mentioned in the supporting information). The parameters derived from the curve fitting are presented in Fig. 3. As a reference, approximate values of the total hydrophilic volume fraction (ϕ_H), calculated as the sum of volume fractions of water plus PEO chains, are also shown. The interaction radius increases almost linearly from approximately 4 to 7 nm as water is added. There is also an increase in the volume fraction of hard spheres. It is noteworthy that the polydispersity decreases when water is added to the system, reaching values below 0.1. However, we should be aware that if the axial ratio of the particles increases, the output polydispersity parameter from GIFT would also increase because elongation mimics polydispersity on the scattering functions $I(q)$. Moreover, the estimated hard-core radius might be smaller than the actual size of micelles due to decreased center-to-center distance between micelles and underestimated volume fraction due to an increased osmotic compressibility with an adhesive interaction between micelles. For hard-sphere suspensions, the maximum packing density is found experimentally to lie near the random close-packed limit of 0.64. A short-

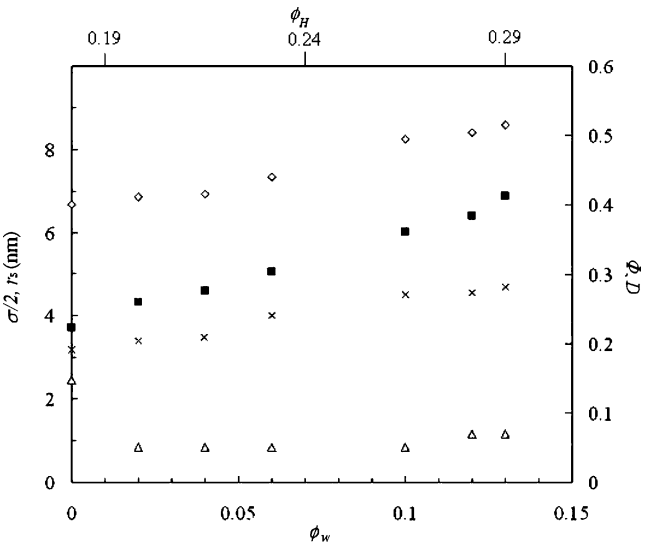

Fig. 3 Parameters estimated from the analysis of $S(q)$ and Pair Distance Distribution Function (PDDF) profiles in SH3775M–D_4–water systems with varying water content at 25 °C. $\sigma/2$ is the interaction radius (*squares*), r_s is the PDDF radius (×), Φ is the hard-sphere volume fraction (*diamonds*), and D is the polydispersity (*triangles*). The total hydrophilic volume fraction ϕ_H is indicated in the *upper horizontal axis*. The SH3775M/D_4 volumetric ratio is 76/24

range adhesive interaction between particles tends to shift this concentration toward higher values because the adhesion creates additional space for particles to move in, owing to the formation of clusters of aggregates. Above the critical volume fraction, the application of the HS model for a fluid-like system is no longer correct. In any case, the estimated values for Φ shown in Fig. 3 are below the critical value.

Figure 4 shows the Pair Distance Distribution Function profiles for different water concentrations. The r-value where $p(r)$ converges to zero gives an estimation of the maximum dimension of the particle, D_{max}. The almost symmetric, bell-shaped curves (especially for systems with added water) suggest a spherical shape for the aggregates, with a radius equal to $r_s=D_{max}/2$. r_s is smaller than the interaction radius (see Fig. 3) at a given water concentration, as expected. The length of an ethylene oxide segment in linear PEO–PDMS reverse aggregates is about 0.3 nm [5]. Assuming that all PEO chains are oriented towards the interior of micellar hydrophilic cores, their radius in the absence of water should be smaller than 5.4 nm, a value estimated from the average chain length PEO groups in the copolymer (n=18). The existence of so-called monomolecular micelles could also be possible as in other graft copolymer systems [24], due to the flexibility of the PDMS backbone. However, the addition of water would favor a larger aggregation number due to micellar swelling and preferential adsorption of copolymer on the nanodroplet interface. Nevertheless, we cannot completely rule out the coexistence of monomolecular and multimolecular micelles, especially in dry systems. On the other hand, we should be aware that at high concentrations, it is sometimes difficult to completely separate the contributions of $P(q)$ and $S(q)$ to the scattering intensity and hence resolve the micellar shape, especially when the contrast is low.

To get more insight on the structure of SH3775M–oil–water systems, we performed rheology measurements. In the absence of water, the viscosity remains constant irrespective of shear rate (see supporting information), indicating Newtonian behavior. When water is added, the samples become non-Newtonian and shear thinning is observed from certain shear rate, which shifts to lower values with the increase in the volume fraction of water. It can be argued that water induces some arrangement between aggregates that is disrupted by shear. Finally, at a water volume fraction ϕ_w=0.12, the viscosity plateau disappears, and the sample shows a yield stress.

In Fig. 5, the value of the viscosity extrapolated to zero-shear rate (η_o) is plotted as a function of ϕ_w. η_o increases exponentially with ϕ_w, and this behavior seems to be almost independent of the kind of oil surrounding the aggregates. It should be pointed out that the value of η_o at ϕ_w=0.12 cannot be properly calculated due to an absence of the plateau at low shear rates, but even a conservative estimation would give a divergence with respect to the trend of Fig. 5, indicating the presence of a glassy transition [25] as the system approaches the critical packing volume fraction. The conditions for our experiments, especially in terms of concentrations, prevent us from making comparisons with models such Dougherty–Krieger or Quemada power-laws, which have been used to describe the viscosity of hard sphere systems [26, 27]. However, the exponential trend of Fig. 5 is in agreement

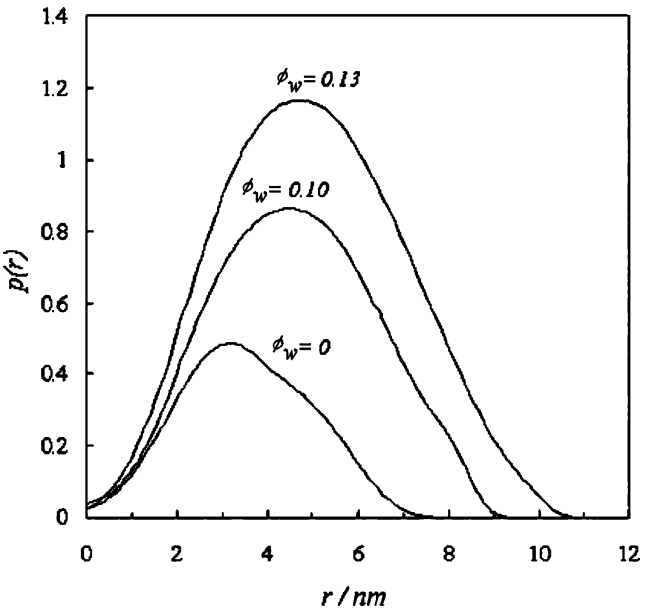

Fig. 4 Pair Distance Distrbution Function [$p(r)$s] for SH3775M–D_4–water systems with varying water content at 25 °C. The SH3775M/D_4 volumetric ratio is 76/24

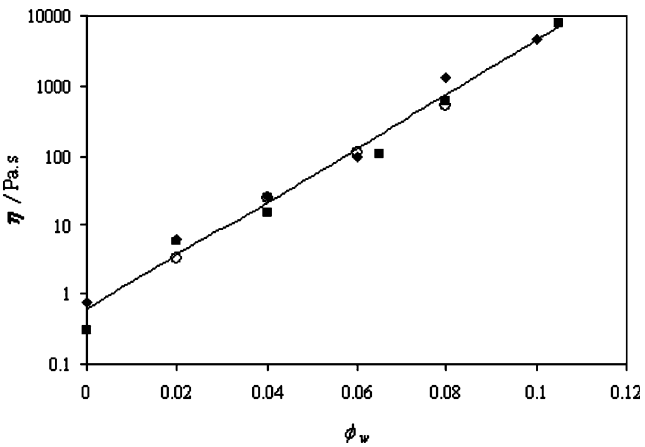

Fig. 5 Viscosity extrapolated to zero-shear as a function of volume fraction of water. *Diamonds* decane, *squares* D_4. The *circles* represent the viscosity of SH3775M–$AgNO_3$ (0.03 M)–D_4 systems after 20 days of preparation. In the last case, ϕ_w represents the volume fraction of $AgNO_3$ (0.03M) in the system

with the Doolittle equation [28], which was found to describe the temperature dependence of liquids approaching the glass transition [29].

Figure 6 shows the results on dynamic rheometry for the samples showing shear thinning. There is a crosspoint between the elastic (G') and viscous (G'') moduli, indicating viscoelastic behavior. At low frequencies, G'' is higher than G' and the system behaves like a liquid, whereas at high frequencies, G'' is lower than G' and the sample behaves like a solid. The fitting of G' data below the crossing point gives a power law $G'=\omega^a$, where ω is the frequency.

In the soft glass rheology (SRG) model [30, 31], the exponent a is related to an effective temperature x that originates from the interactions between the different entities. Below the glass transition, $x<1$. Above the glass transition, and for $1<x<3$, $G'=\omega^{x-1}$. When $x>3$, $G'=\omega^2$ and the system behaves according to the Maxwell model. The values of a are listed in Table 1 as a function of water content, and it is observed that all values are lower than two; therefore, the behavior is non-Maxwellian, suggesting multiple relaxation times. It can also be seen in Table 1 that values of x estimated by the SRG model decrease as water is added, indicating that the system approaches and even passes the glass transition [32].

The inverse of the value of frequency at the crossing point ($1/\omega_c$) is representative of the relaxation dynamics of the system; namely, relaxation is slower for smaller values of ω_c. Therefore, the shifting of ω_c to lower values with the incorporation of water in the system suggests an increase in relaxation times, and finally, the cross point disappears from the experimental range and G' becomes almost frequency-independent (see the low value of a in Table 1); hence, there is gel-like behavior. It should be pointed that there is phase separation for $\phi_w>0.14$.

Table 1 Exponent of the power law $G'=\omega^a$ and effective temperature x (SRG model) as a function of φ_w

ϕ_w	a	x
0.08	1.90	2.90
0.10	1.64	2.64
0.12	1.22	2.22
0.14	0.12	1.12

Synthesis of silver nanoparticles

Reverse micellar systems described above were used for the synthesis of silver nanoparticles by solubilizing $AgNO_3$(aq.) inside the reverse aggregates. As the reaction proceeded, the color of the samples, initially colorless, changed to yellow or to brown. No precipitation was observed, indicating that particles were well dispersed.

The formation of silver nanoparticles was followed by UV spectrometry. Figure 7a shows the results of time-resolved measurements. Initially, there is a very broad but still detectable band around 430 nm, indicating that in the time gap between mixing and placing the sample in the spectrophotometer, there is already some reduction of silver taking place. With the course of time, the intensity of the band increases and the position of the maximum suffers a slight blue shift to 420 nm, which has been observed in similar studies [33]. This wavelength is characteristic of the plasmon band of silver [33]. No significant change in the band width at half of the maximum was observed, which implies that the particle size remains almost uniform in the time scale of the experiment. Therefore, the increase in the intensity of the plasmon band is mainly associated with an increase in the number density of particles. Note that there is also a small band or shoulder at around 290 nm, which is attributed to the presence of small Ag atomic clusters [34, 35].

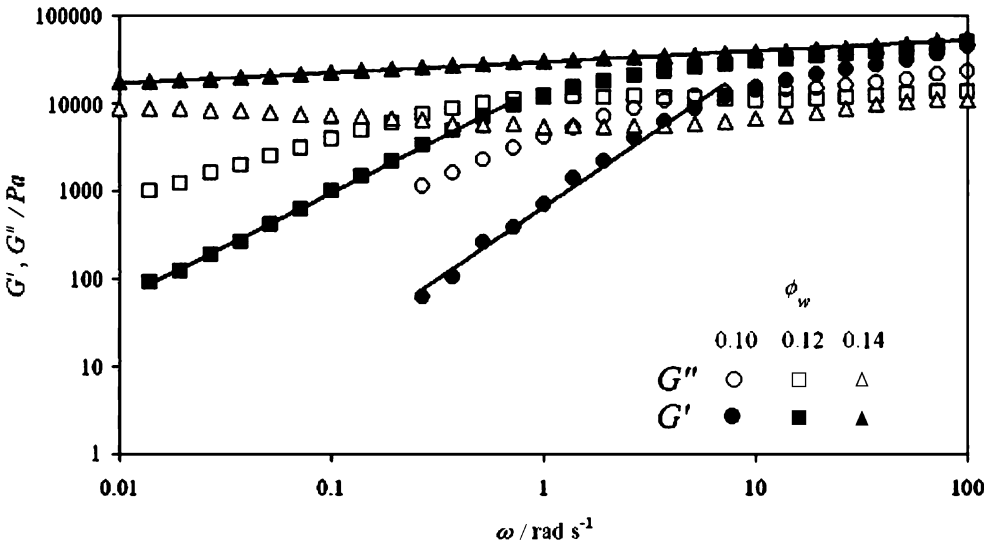

Fig. 6 Dynamic rheological measurements of SH3775M–D_4–water systems for different volume fractions of water. G' is the elastic modulus and G'' is the viscous modulus. *Lines* are best fits to the data below the crossing frequency. The SH3775M/D_4 volumetric ratio is 76/24

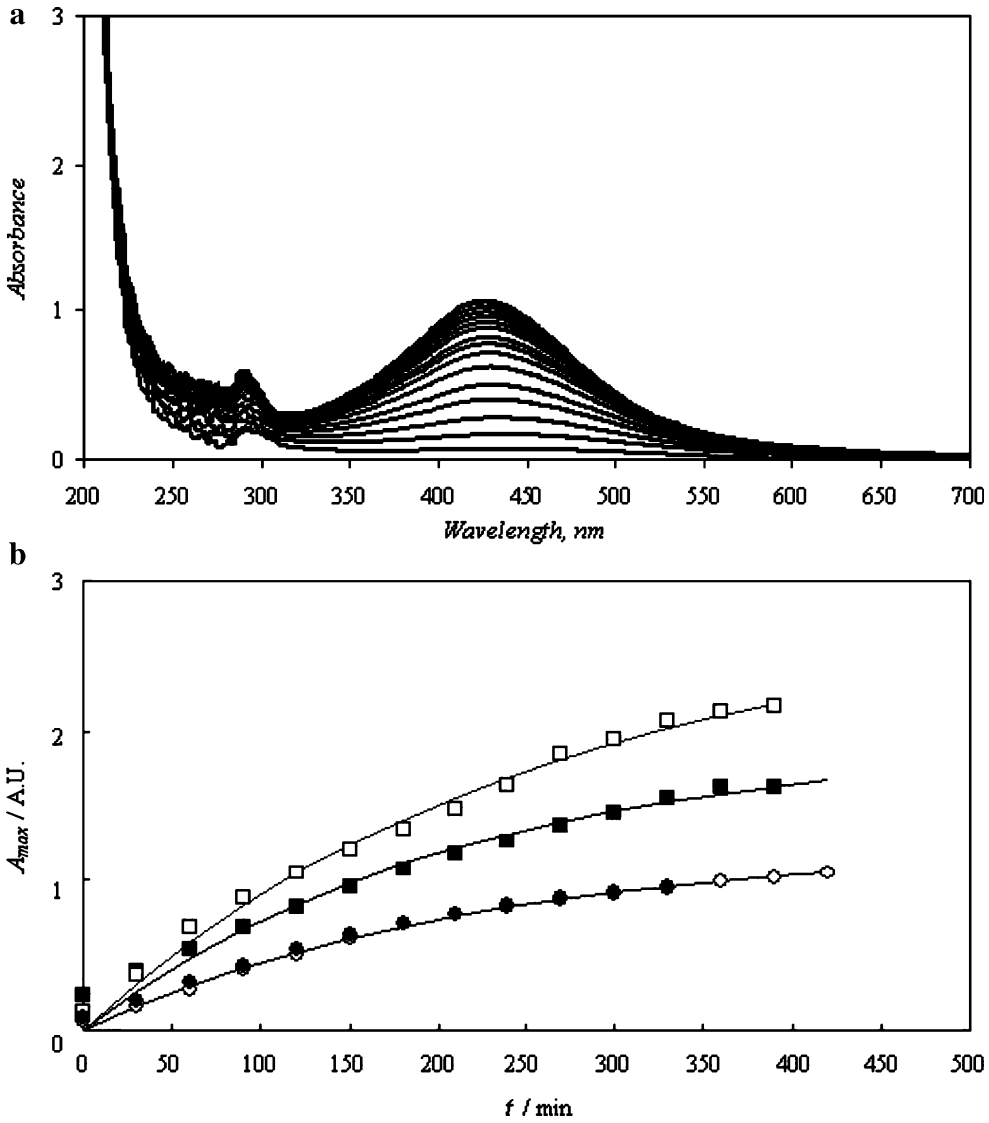

Fig. 7 **a** Representative UV spectra for SH3775M–$AgNO_3$ (0.03 M)–D_4 samples as a function of time. Spectra were collected every 30 min. The SH3775M–water–D_4 ratio is 77/23 and the initial $AgNO_3$ (0.03M) contents is 2 wt.%. **b** Change of the absorbance at the maximum of Ag plasmon band as a function of time. The SH3775M/oil weight ratio is 77/23 and the initial $AgNO_3$ (0.03M) contents are 2 wt.% (*circles*) and 6 wt.% (*squares*). *Open* and *filled symbols* correspond to D_4 and decane systems, respectively. *Lines* are best fits to Eq. 1

On the other hand, it was observed that the intensity of the plasmon band increases with $AgNO_3$ content. As no reducing agent was added to the system, it seems that some groups of SH3775M molecule, most probably the ethylene oxide chains facing the interior of micelles solubilizing $AgNO_3$(aq.), induce the reduction of Ag ions

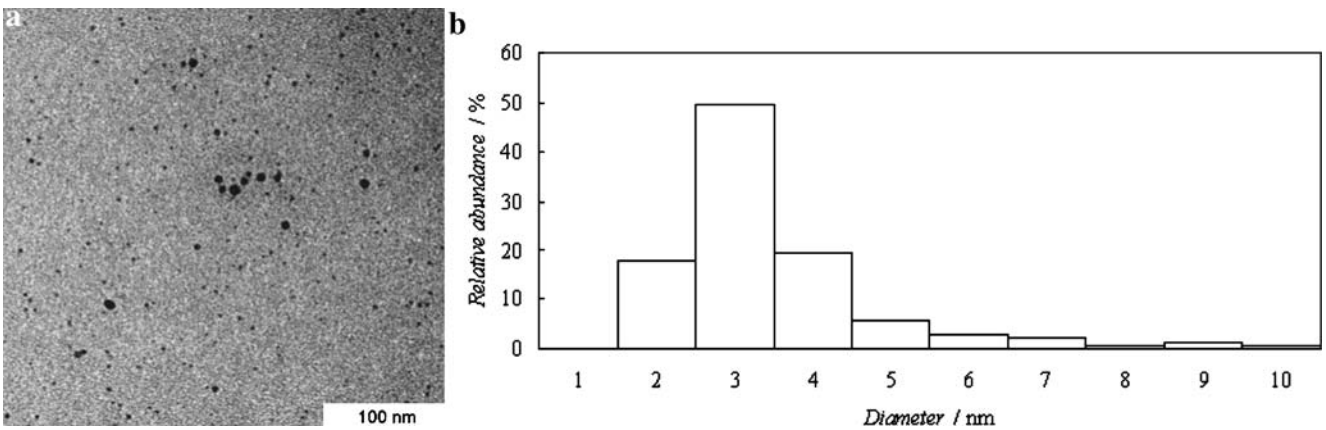

Fig. 8 **a** Representative TEM picture of silver nanoparticles produced from SH3775M–$AgNO_3$ (0.03 M)–D_4 mixtures after 10 h. **b** Size distribution of silver nanoparticles from TEM

to metallic silver, similar to the case of nonionic surfactants [36–38]. Although the reduction is possibly facilitated via metal ion complexation with PEO segments to form pseudo crown ether structures [39], a direct reducing action of macroradicals formed during the degradation of the polymer cannot be excluded, e.g., as recently proposed for the synthesis of silver hydrosols with poly(*N*-vinyl-2-pirrolidone) [40].

To follow the kinetics of nanoparticle formation, the change of the absorbance at the maximum of Ag plasmon band (A_{max}) as a function of time is presented in Fig. 7b. As in the synthesis of silver nanoparticles using nonionic surfactant [41], there is a good fit to a first-order rate equation given by:

$$A_{max} = A_{\infty}(1 - \exp(-k_1 t)) \quad (1)$$

where A_{∞} is the absorbance at relatively long times and k_1 is a rate constant. From curve fittings, k_1 is estimated to be around 4×10^{-3} min^{-1} for the examined samples, which is within the same order of magnitude that the values obtained using polyoxyethylene-type nonionic surfactants [38].

At low initial $AgNO_3$(aq.) contents, the curves for D_4 and decane systems almost coincide. However, as the $AgNO_3$(aq.) content is increased, A_{max} values and their rate of change are higher for D_4 systems. The reasons for this the difference are still obscure and will be the subject of future investigations. No significant effects of nanoparticle formation on the rheology of the system were found (see Fig. 5); namely, the viscosity increases with the fraction of the dispersed phase in the same fashion as the systems discussed in the first part of this section, which gives an indication that silver nanoparticles are embedded within a viscoelastic structure that has not been disrupted during the synthesis.

Figure 8 shows additional data on silver nanoparticles. Using Transmission Electron Microscopy (TEM), spherical particles were observed (the same shape estimated for reverse micelles), and the particle size was mostly below 10 nm, with a maximum centered around 3–4 nm (Fig. 8b), obtained from a particle population over 100. Similar to TEM results, the size distribution estimated from dynamic light scattering (see supporting information) is asymmetric but is shifted to higher sizes because the value of the hydrodynamic radius is influenced by the polymer chains attached to the particles and their solvation. The radius of silver nanoparticles is smaller than that of SH3775M micelles derived from SAXS analysis (Fig. 3). However, we should take into account that particles would be preferentially formed in the core of micelles where there is an aqueous pool free of PEO chains. Namely, the length of PEO chains should be subtracted from the micellar diameter to estimate the effective space available for particle formation. From the value of r_s in the absence of water (Fig. 3), the length of the PEO chain is calculated to be about 3 nm. Using this value and that of r_s at ϕ_w similar to the concentration of $AgNO_3$(aq.) in Fig. 8, a rough estimation would give a diameter of around 2 nm for the water pool. Hence, it seems that the size of micellar cores and nanoparticles are similar, and therefore, copolymer aggregates might be acting as templates. This hypothesis is supported by the fact that there was no significant change in the SAXS patterns for samples containing silver nanoparticles, as compared with those in the absence of silver, which provides evidence that the structure of reverse micelles (which contributes most to the scattering at low angles) is preserved, in agreement with rheology results.

Conclusions

Reverse micelles are formed by PDMS-graft-poly(oxyethylene) copolymer SH3775M dissolved in nonpolar solvents. The micelles swell upon solubilization of water inside the aggregates, producing an increase in viscosity and the appearance of viscoelastic behavior, although there is no ordered packing. Silver nanoparticles can be synthesized using the aggregates as nanoreactors and templates, without the aid of additional reducing agent, so that nanoparticles embedded in a viscoelastic matrix are obtained.

Acknowledgment The authors are grateful to Dr. Takaaki Sato (Waseda University, Japan) for useful discussions and suggestions on SAXS results, and to Dr. Dominique Scalarone (University of Torino, Italy), for providing data on size-exclusion chromatography.

References

1. Schmidt GLF (1973) In: Karsa DR (ed) Industrial applications of surfactants. Royal Society of Chemistry, London, p 24
2. He M, Hill RM, Lin Z, Scriven LE, Davis HT (1993) J Phys Chem 97:8820
3. Hill RM, He M, Lin Z, Davis HT, Scriven LE (1993) Langmuir 9:2789
4. Rodríguez C, Uddin Md H, Watanabe K, Furukawa H, Harashima A, Kunieda HJ (2002) Phys Chem B 106:22
5. Uddin MH, Rodríguez C, López-Quintela MA, Tarrazo T, Solans C, Esquena J, Kunieda H (2003) Macromolecules 36:1261
6. Soni SS, Sastry NV, Aswal VK, Goyal PSJ (2002) Phys Chem B 106:2606
7. Lin Y, Alexandridis P (2002) J Phys Chem B 106:10845
8. Wanatabe K, Kanei N, Kunieda H (2002) J Oleo Sci 51:771
9. Hill RM (1997) In: Robb ID (ed) Specialist surfactants. Blackie Academic and Professional, London
10. Gradzielski M, Hoffmann H, Robisch P, Ulbricht W (1990) Tenside Surf Deterg 27:366
11. Stuermer A, Thunig C, Hoffmann H, Gruening B (1994) Tenside Surf Deterg 31:90
12. Hill RM (1999) Silicone surfactants, surfactant sci series 86. Marcel Dekker, New York

13. Xu AW, Yu JC, Cai YP, Zhan HX, Zhang LZ (2002) Chem Commun 1614
14. Michaut F, Hebraud P, Lafuma F, Perrin P (2003) Langmuir 19:10086
15. Lopez-Quintela MA (2003) Curr Opin Colloid Interface Sci 8:137
16. Lazzari M, Lopez-Quintela MA (2003) Adv Mater 15:1583
17. Lazzari M, Rodríguez C, Rivas J, López-Quintela MA (2006) J Nanosci Nanotechnol 6:892
18. Zhang R, Liu J, Han B, He J, Liu Z, Zhang J (2003) Langmuir 19:8611
19. Sakai T, Alexandridis P (2006) Chem Mater 18:2577
20. Lei Z, Fan Y (2006) Mater Lett 60:2256
21. Kaito A, Tanigaki N, Kyotani H, Shimomura M (2001) Macromol Mater Eng 286:369
22. Neugebauer D, Zhang Y, Pakula T, Matyjaszewski K (2005) Macromolecules 38:8687
23. Lopez-Quintela MA, Akahane A, Rodriguez C, Kunieda H (2002) J Colloid Interface Sci 247:186
24. Kikuchi A, Nose T (1996) Macromolecules 29:6770
25. Meeker SP, Poon WCK, Pusey PN (1997) Phys Rev E 55:5718
26. Goodwin JW, Ottewill RH (1991) J Chem Soc Faraday Trans 87:357
27. Weiss A, Dingenouts N, Ballauff M, Senff H, Richtering W (1998) Langmuir 14:5083
28. Doolittle AK, Doolittle DB (1957) J Appl Phys 28:901
29. Marshall L, Zukoski CF (1990) J Phys Chem 94:1164
30. Sollich P, Lequeux F, Hebraud P, Cates M (1997) Phys Rev Lett 78:2020
31. Sollich P (1998) Phys Rev E 58:738
32. Bonn D, Coussot P, Huynh HT, Bertrandand F, Debregeas G (2002) Europhys Lett 59:786
33. Petit C, Lixon P, Pileni M-P (1993) J Phys Chem 97:12974
34. Linnert T, Mulvaney P, Henglein A, Weller HJ (1990) J Am Chem Soc 112:4657
35. Rodríguez-Sanchez ML, Rodríguez MJ, Blanco MC, Rivas J, López-Quintela MA (2005) J Phys Chem B 109:1183
36. Barnickel P, Wokaun A (1990) Mol Phys 69:1
37. Currie F, Andersson M, Holmberg K (2004) Langmuir 20:3835
38. Andersson M, Pedersen JS, Palmqvist AEC (2005) Langmuir 21:11387
39. Sakai T, Alexandridis P (2005) Langmuir 21:8019
40. Hoppe CE, Lazzari M, Pardiñas-Blanco I, López-Quintela MA (2006) Langmuir 22:7027
41. Liz-Marzán LM, Lado-Touriño I (1996) Langmuir 12:3585